Applied Catalysis B: Environmental 209 (2017) 637–647

Contents lists available at ScienceDirect

Applied Catalysis B: Environmental

journal homepage: www.elsevier.com/locate/apcatb

Kinetics of oxidative degradation/mineralization pathways of the antibiotic tetracycline by the novel heterogeneous electro-Fenton process with solid catalyst chalcopyrite

Natija Barhoumi[a,b], Hugo Olvera-Vargas[b], Nihal Oturan[b], David Huguenot[a,b,c,d], Abdellatif Gadri[e], Salah Ammar[e], Enric Brillas[d], Mehmet A. Oturan[b,*]

[a] Département de chimie Faculté des Sciences de Gabès, Cité Erriadh, Université de Gabès, 6027 Gabès, Tunisia
[b] Université Paris-Est, Laboratoire Géomatériaux et Environnement, EA 4508, UPEM, 5 Bd Descartes, 77454 Marne-la-Vallée, Cedex 2, France
[c] Département de chimie Faculté des Sciences de Bizerte, Cité Zarzouna, Université de Carthage, Tunisia
[d] Laboratori d'Electroquímica dels Materials i del Medi Ambient, Departament de Química Física, Facultat de Química, Universitat de Barcelona, Martí i Franquès 1-11, 08028 Barcelona, Spain
[e] Unité de recherche Electrochimie, Matériaux et Environnement UREME (UR17ES45), Faculté des Sciences de Gabès, Université de Gabès, Cité Erriadh, 6072 Gabès, Tunisie

ARTICLE INFO

Article history:
Received 15 January 2017
Received in revised form 26 February 2017
Accepted 9 March 2017
Available online 11 March 2017

Keywords:
Heterogeneous catalysis
Chalcopyrite
Electro-Fenton
Tetracycline
Wastewater treatment

ABSTRACT

The degradation of solutions of the antibiotic tetracycline (TC) has been studied by a novel electrochemical advanced oxidation process, consisting in electro-Fenton (EF) process using chalcopyrite as heterogeneous catalyst. In fact, chalcopyrite powder was the source of Fe^{2+} and Cu^{2+} ions instead of a soluble catalyst salt used in conventional EF. Experiments were performed in an undivided cell equipped with a Pt or boron-doped diamond (BDD) anode and a carbon felt cathode, where TC and its oxidation intermediate products were destroyed by hydroxyl radicals (•OH) formed both, in the bulk solution from electrochemically induced Fenton's reaction (Fe^{2+} and H_2O_2) and Fenton's-like reaction (Cu^{+} and H_2O_2), and at the anode surface from water oxidation. The effects of operating parameters such as applied current, chalcopyrite concentration and anode material were investigated. TC decay followed pseudo-first-order reaction kinetics. The absolute rate constant for TC oxidation by •OH was found to be 3.2×10^9 M^{-1} s^{-1}, as determined by the competition kinetic method. EF process using chalcopyrite as heterogeneous catalyst showed to be more efficient than conventional EF, achieving almost total mineralization of the TC solution (98% of total organic carbon removal) after 360 min under optimum operating conditions. A plausible mineralization pathway for mineralization of TC aqueous solution by •OH was proposed based on the identification of different oxidation by-products. Moreover, toxicity tests pointed out that this heterogeneous EF process was able to detoxify the TC solutions.

1. Introduction

The presence of pharmaceuticals in the aquatic environment is now well recognized as an important issue, causing long-term adverse impacts on the ecosystems and human health [1,2]. Pharmaceutical industries, hospitals and urban wastewater effluents are important points of drug discharge into the environment, leading to a significant effect on the physical, chemical and biological composition of water bodies [3]. Among drugs, antibiotics are widely used in human and veterinary medicine to treat diseases. The presence of low levels of antibiotics and their transformation products in the environment could have adverse effects, such as bacterial resistance and disruption of key cycles critical to aquatic ecology or crop and animal production [4,5]. Because of their recalcitrant character, antibiotics, and drugs in general, are ineffectively removed in conventional wastewater treatment plants [2,5,6]. Nevertheless, advanced oxidation processes (AOPs) have proved to be a suitable alternative for rapid degradation of recalcitrant and non-biodegradable compounds in water [7,8]. Among them, electrochemical advanced oxidation processes (EAOPs) have received great attention over the last decade as an effective and suitable technology for the remediation of wastewater contaminated with toxic and persistent organic pollutants [9–11].

* Corresponding author.
E-mail addresses: mehmet.oturan@univ-paris-est.fr, mehmet.oturan@u-pem.fr (M.A. Oturan).

http://dx.doi.org/10.1016/j.apcatb.2017.03.034
0926-3373/

One of the most attractive EAOPs is the electro-Fenton process (EF), in which H_2O_2 is formed by the two-electron reduction of dissolved O_2 (Eq. (1)) at a suitable carbonaceous cathode, such as graphite, carbon felt, reticulated vitreous carbon, gas diffusion electrodes (GDE), boron-doped diamond (BDD), carbon nanotubes, activated carbon fiber, and so on [12–18].

$$O_2 + 2H^+ + 2e^- \rightarrow H_2O_2 \quad (1)$$

In acidic medium, the oxidizing power of H_2O_2 is strongly enhanced by the addition of a catalytic amount of Fe^{2+} (or Fe^{3+}) ions, which promotes the generation of homogeneous $^{\bullet}OH$ via Fenton's reaction (Eq. (2)). Furthermore, Fe^{2+} ions are rapidly regenerated from reduction of Fe^{3+} ion at the cathode according to Reaction (3) [12].

$$Fe^{2+} + H_2O_2 + H^+ \rightarrow Fe^{3+} + H_2O + {}^{\bullet}OH \quad (2)$$

$$Fe^{3+} + e^- \rightarrow Fe^{2+} \quad (3)$$

When a non-active anode material (M) with a high O_2 evolution overpotential such as BDD is used in EF process, heterogeneous M($^{\bullet}OH$) radicals are also formed at the anode surface by water oxidation (Eq. (4)), whence enhancing the efficiency of the process [19,20]. BDD electrodes are currently the most powerful and preferred anodes for electrochemical oxidation [10,21,22].

$$M + H_2O \rightarrow M({}^{\bullet}OH) + H^+ + e^- \quad (4)$$

EF process is typically performed using soluble ferric salts as catalyst (Fe^{2+}) source. However, other transitions metals have also been used to promote Fenton like reaction, such as Cu^{2+} ions, showing good results [23,24]. On the other hand, the use of alternative heterogeneous catalyst has been proposed aiming to enhancing the effectiveness of Fenton's-based processes with parallel sustainability purposes. These "green" catalysts containing Fe and/or Cu solids include pyrite (FeS_2), chalcocite (Cu_2S), bornite (Cu_5FeS_4), magnetite (Fe_2O_3) or wustite (FeO) [25–28].

On the other hand, the chalcopyrite is one of the most important copper sulfide minerals in the world [29,30]. It can releases Cu^{2+} and Fe^{2+} ions in aqueous solution according to Reactions (5)–(7) [30]. In the present work, we explore the novel possibility of using this mineral for catalyzing the EF process (EF/Chalcopyrite) during the degradation of synthetic aqueous solutions of antibiotic tetracycline (TC).

$$CuFeS_{2(s)} + 4O_2 \rightarrow Cu^{2+} + Fe^{2+} + 2SO_4{}^{2-} \quad (5)$$

$$CuFeS_{2(s)} + 4H^+ + O_2 \rightarrow Cu^{2+} + Fe^{2+} + 2S^0_{(s)} + 2H_2O \quad (6)$$

$$CuFeS_{2(s)} + 16Fe^{3+} + 8H_2O \rightarrow Cu^{2+} + 17Fe^{2+} + 2SO_4{}^{2-} + 16H^+ \quad (7)$$

In addition of self-regulation of catalyst, chalcopyrite allows also the self-regulation of solution pH. Taking into account that pH values around 3 constitute the optimum values for Fenton's reaction, reaction (Eq. (7)) becomes highly important being as the release of H^+ contributes to the acidification of the solution, thus the use of mineral acids for pH adjustment becomes unnecessary.

TC is an antibiotic extensively used for disease control due to their great therapeutic values. It is also widely used in livestock feed to prevent illness and promote growth. Its detection in aquatic systems and soils has raised concern about its biological impacts and potential risks to the environment, as well as to public health [31]. Due to its large global consumption, it was chosen as a model molecule for assessing the efficiency of the innovative EF/Chalcopyrite heterogeneous process.

Interestingly, in a recent study, synthesized chalcopyrite nanocrystals supported on sawdust were applied for the degradation of organic dyes in a filtration column in which H_2O_2 was externally supplied [32]. Although high efficiency was obtained for the discoloration of dye solutions (via Fenton's reaction), any data on mineralization of the dyes to CO_2, H_2O and inorganic ions was not reported. However, these results highlighted the potential of chalcopyrite as catalyst for Fenton-based processes, among which EF presents several advantages as discussed above.

This work hence presents a thorough assessment of the performance of the EF/Chalcopyrite process through examination of the main operating parameters affecting degradation and mineralization efficiencies, such as catalyst concentration, applied current, and the effect of the anode material. Additionally, a comparative study with homogeneous EF using Fe^{2+} and Cu^{2+} ions as catalyst is presented. The identification of aromatic intermediates, as well as short-chain carboxylic acids and inorganic ions formed during EF/Chalcopyrite treatment of TC, allowed the proposal of a mineralization pathway of the drug with $^{\bullet}OH$. Moreover, toxicity evaluation throughout electrolysis by means of the Microtox method is presented.

2. Materials and methods

2.1. Chemicals

Analytical grade TC ($C_{22}H_{24}N_2O_8$) with purity >98%, was purchased from Fluka and was used in the electrolytic experiments without further purification. Anhydrous sodium sulphate, used as background electrolyte, as well as H_2SO_4 and NaOH were provided from Acros Organics. Heptahydrated iron (II) sulphate and copper (II) sulphate pentahydrate used as catalysts in conventional EF were of analytical grade from Acros Organics. All solutions were prepared with ultrapure water from a Millipore Milli-Q system (Molsheim, France) with resistivity >18 MΩ cm^{-1}. Carboxylic acids were of reagent grade supplied by Sigma-Aldrich and Merck.

The sonication was made in a BRANSON 2510 equipment with 40 kHz frequency and 237 W energy intensity.

2.2. Characterization of chalcopyrite powder

Chalcopyrite ($CuFeS_2$) used in this work was mined from Tunisia. It was milled with a ceramic mortar and sieved (<80 μm). To remove surface impurities, the resulting powder was ultrasonicated in 95% ethanol for 5 min (using a BRANSON 2510 equipment with 40 KHz frequency and 237 W energy intensity) and then washed with 1 M HNO_3, rinsed with deionized water, further with 95% ethanol and finally dried at 30 °C. Table 1 collects the composition found by inductively coupled plasma spectrometry (ICP) analysis of the powder dissolved in 16 M HNO_3. The great purity of the sample prepared with 1 g L^{-1} in mass of $CuFeS_2$, corresponding to 27% in mass of iron and 21% in mass of copper, is worth noting. The crystal structure of chalcopyrite powder was characterized by X-ray diffraction (XRD) using a SIEMENS D5000 diffractometer with secondary graphite monochromator and CuKα radiation. XRD spectrum depicted in Fig. 1, shows a series of peaks, which are in

Table 1
Chemical composition of the chalcopyrite powder used in this study.

Element	Fe	Cu	S	Zn	Pb	Al	Cd	Cr	Ni	Co	Mn	Ca	Mg
Mass (%)	27.03	21.0	47.72	0.25	0.49	0.52	0.31	0.25	0.26	0.25	0.45	0.97	0.49

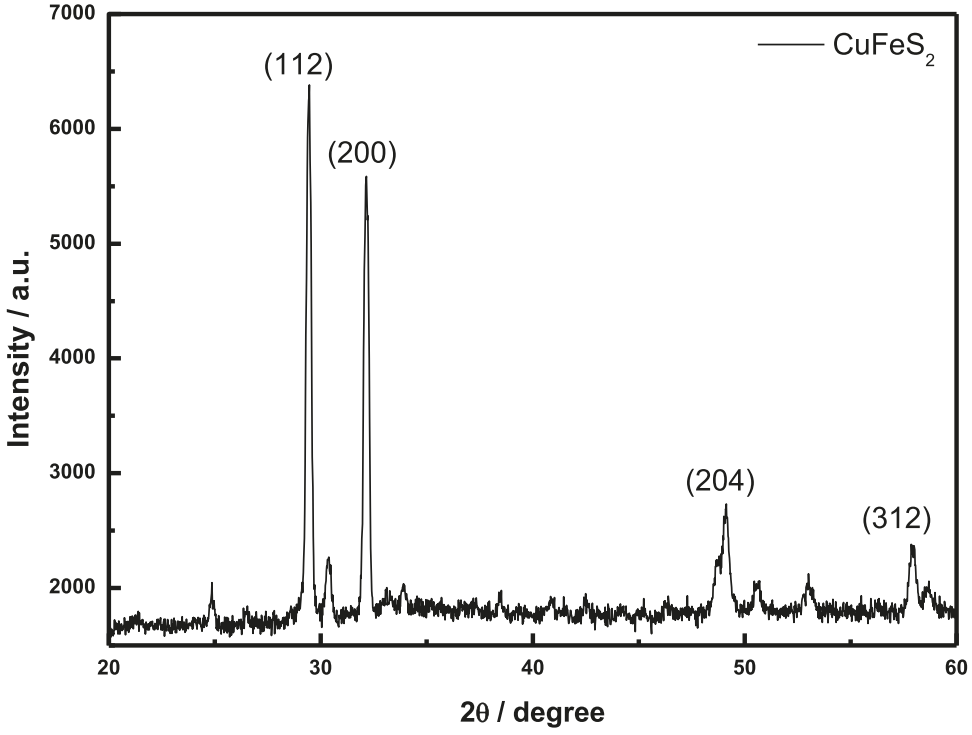

Fig. 1. XRD spectrum of chalcopyrite used in this study.

agreement with those of crystallographic planes reported by the ICDD 83-0983 [33].

2.3. EF/Chalcopyrite treatment

All electrolyses were carried out in an undivided cylindrical cell containing 230 mL solutions under vigorous stirring with a magnetic bar. The anode was a cylindrical Pt mesh of 4.5 cm height and 3 cm internal diameter from Goodfellow (Lille, France) or a 25 cm^2 thin-film BDD onto a Nb substrate from Condias Gmbh (Itzehoe, Germany). The cathode was 3D carbon felt piece (15 cm × 4 cm × 0.5 cm) from Carbon-Lorraine (Paris, France). The anode was always centred in the electrochemical cell and was surrounded by the cathode, which covered the inner wall of the cell. The solution was continuously aired at a flow of 1 L min^{-1} starting 10 min before the beginning of electrolysis and during the whole duration. Electrolyses were performed using 0.20 mM (89 mg L^{-1}) TC solutions in 0.050 M Na_2SO_4 with amounts of chalcopyrite ranging between 0.5–2.0 g L^{-1}, at natural initial pH (5.94) and room temperature, by applying constant current between 50–500 mA. The experiments were conducted in the dark covering the cell with an aluminium paper to avoid any photolytic effect. The corresponding cell voltage ranged between 3.6–5.6 V from 50 to 500 mA, respectively. The catalyst was easily recovered at the end of treatment by filtration. Concerning the EF process, pH of the solutions was adjusted to a value of 3 with H_2SO_4 before experiments, and $FeSO_4$ was added as catalyst at 0.10 mM concentration [34].

2.4. Apparatus and analytical procedures

The pH of solutions was measured with a CyberScan pH 1500 pH-meter from EuTech Instruments (Singapore). The mineralization of TC solutions was assessed from their TOC decay determined on a VCSH TOC analyser from Shimadzu (Marne-La-Vallée, France). TOC removal values were then utilized for determining the mineralization current efficiency (MCE) at current I (in A) that was estimated by Eq. (8) [12]:

$$\mathrm{MCE}(\%) = \frac{nFV_s\Delta(\mathrm{TOC})_{\mathrm{exp}}}{4.32\times10^7 mIt}\times 100 \quad (8)$$

where F is the Faraday constant (96,485 C mol^{-1}), V_s is the solution volume (in L), $\Delta(\mathrm{TOC})_{\mathrm{exp}}$ is the experimental TOC decay (in mg L^{-1}), 4.32×10^7 is a conversion factor to homogenize units (=3600 s h^{-1} × 12000 mg of C mol^{-1}), m is the number of carbon atoms of TC (=22) and t is the electrolysis time (h). The number of electrons n consumed per TC molecule during its mineralization was taken as 90, according to the mineralization Reaction (9), with the assumption that most of the N contained in TC was transformed into NH_4^+ [35].

$$C_{22}H_{24}N_2O_8 + 36H_2O \rightarrow 22CO_2 + 2NH_4^+ + 88H^+ + 90\,e^- \quad (9)$$

The time-course of TC concentration was followed by reversed-phase HPLC using a Merck Lachrom LC fitted with a RP-18 (5 μm, 250 mm × 4.6 mm) column from VWR International (Fontenay-sous-Bois, France) at 40 °C, and coupled with a L-7455 UV–vis detector from Hitachi, selected at λ = 275 nm. Analyses were carried out in isocratic mode, with a solvent mixture of 79.5:19.5:1 (v/v/v) water/methanol/acetic acid as a mobile phase at a flow rate of 0.8 mL min^{-1}. Generated aliphatic acids were followed by ion-exclusion HPLC using an Altech (Andhra Pradesh, India) LC fitted with a Supelcogel H (9 μm, 25 cm × 4.6 mm) column from Supelco (Saint-Quentin Fallavier, France) at room temperature, and coupled with an AD20 UV detector from Dionex (Courtaboeuf, France) set at λ = 210 nm, and using 1% H_2SO_4 at 0.2 mL min^{-1} as mobile phase. The released inorganic ions were detected by ion chromatography using a Dionex ICS-1000 Basic Ion Chromatography System coupled with a Dionex DS6 conductimetric detector containing a cell at 35 °C. NH_4^+ content was determined with a Dionex CS12A (25 cm × 4 mm) cation column, with a mobile phase of 9.0 mM H_2SO_4 at 1.0 mL min^{-1}. NO_3^- content was measured with a Dionex AS4A-SC (25 cm × 4.6 mm) anion column, using

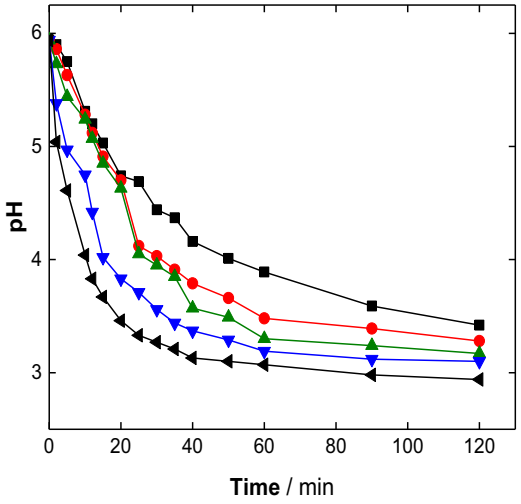

Fig. 2. Time-course of pH for 230 mL of 0.050 M Na_2SO_4 with chalcopyrite powder in suspension by bubbling compressed air at 1 L min^{-1}. BDD/carbon-felt cell, $[Chalcopyrite]_0$: (■) 0.25 g L^{-1}, (●) 0.5 g L^{-1}, (▲) 0.75 g L^{-1}, (▼) 1.0 g L^{-1} and (◄) 2.0 g L^{-1}.

a 1.8 mM Na_2CO_3 + 1.7 mM $NaHCO_3$ solution at 2.0 mL min^{-1} as mobile phase.

Cyclic organic products formed during EF/Chalcopyrite were identified by:

(1) GC–MS, using a Thermo Finnigan PolarisQ instrument (EI mode, 70 eV) equipped with a TRB-5-MS column from Teknokroma. He was used as carrier gas at 1.5 mL min^{-1}. The column was initially held at 40 °C for 2 min, afterwards the temperature was increased to 280 °C at a rate of 10 °C min^{-1}, and kept at this temperature for 4 min. Liquid–liquid extraction with ethyl acetate was made before analysis, as well as derivatization with N,O-Bis (trimethylsilyl) trifluoroacetamide (99%).
(2) HPLC–MS, using a Nexera UHPLC LC coupled with a MS2020 simple quadrupole mass spectrometer from Shimadzu, utilizing atmospheric pressure chemical ionization (APCI). The column was a Kinetex 2.7 μm, C18 100 Å, 100 mm × 2.1 mm. Eluted compounds were detected between m/z 50 and 600. The mobile phase consisted of: methanol including 0.01% formic acid (A), and water with 0.01% formic acid (B), while the elution program at 0.5 mL min^{-1} was the following: 0–2 min (isocratic 5/95), 2–7 min (gradient up to 80/20), 7–8 min (isocratic 80/20).

3. Results and discussion

3.1. Properties of aqueous solutions with chalcopyrite powder in suspension

Before applying the EF/Chalcopyrite process to removal of TC, preliminary experiments were performed in order to study the properties of chalcopyrite in aqueous solutions. Fig. 2 shows the change in pH starting from the natural pH value of TC solution (near 5.94), varying the initial load of chalcopyrite slurry from 0.25 to 2.0 g L^{-1}. In all cases, the solution pH progressively dropped, reaching values between 4.69 and 3.33 within 25 min. It further declined reaching values in the range of 3.42–2.94 after 120 min. Fe^{2+} and Cu^{2+} ions were released into the solution. Both of them catalyse H_2O_2 decomposition leading to formation of •OH; Fe^{2+} through Fenton's reaction (2), and Cu^{2+} via Fenton-like reaction (13). To take place this reaction, Cu^{2+} is previously reduced both, at the cathode by Reaction (10), and in the bulk according to Reactions (11) and (12). Moreover, Cu^{+} contributes to regeneration of

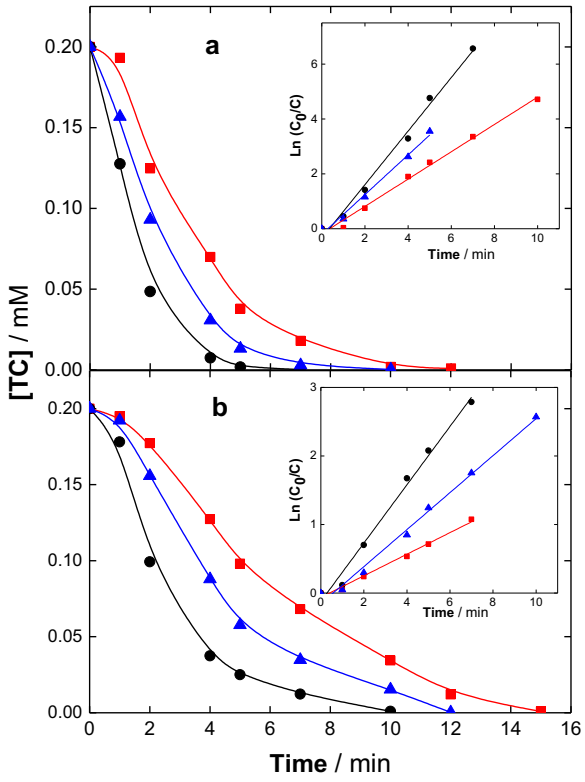

Fig. 3. Effect of chalcopyrite dosage on the oxidative degradation of 230 mL of 0.20 mM antibiotic TC during EF/chalcopyrite process, using 0.050 M Na_2SO_4 at 300 mA and 25 °C in undivided cells: (a) BDD/carbon-felt and (b) Pt/carbon-felt. $[Chalcopyrite]_0$: (■) 0.5 g L^{-1}, (●) 1.0 g L^{-1} and (▲) 2.0 g L^{-1}. Inset panels show the kinetics analysis as a pseudo-first-order reaction.

Fe^{2+} according to Reaction (15), which propagates Fenton's reaction [12,24,36]. We hypothesized that Reactions (5)–(7) reach an equilibrium state that explains the final steady pH values attained for each concentration of chalcopyrite (Fig. 2). These results highlight that favourable pH value for electro-Fenton process can be obtained from a chalcopyrite dosage of 1.0–2.0 g L^{-1}.

$$Cu^{2+} + e^- \rightarrow Cu^+ \quad (10)$$

$$Cu^{2+} + H_2O_2 \rightarrow Cu^+ + HO_2^{\bullet} + H^+ \quad (11)$$

$$Cu^{2+} + HO_2^{\bullet} \rightarrow Cu^+ + H^+ + O_2 \quad (12)$$

$$Cu^+ + H_2O_2 \rightarrow Cu^{2+} + {}^{\bullet}OH + OH^- \quad (13)$$

$$Cu^+ + Fe^{3+} \rightarrow Cu^{2+} + Fe^{2+} \quad (14)$$

3.2. Effect of chalcopyrite concentration on TC degradation

It is well known that catalyst concentration plays a fundamental role in the efficiency of EF process. In order to clarify the effect of concentration chalcopyrite of concentration on TC decay, 230 mL of 0.20 mM antibiotic solution were treated by EF with BDD anode (EF-BDD/Chalcopyrite) and by Pt anode (EF-Pt/Chalcopyrite), varying catalyst dosage (chalcopyrite mass per L of solution) in the range of 0.5–2.0 g L^{-1}, at 300 mA.

Fig. 3a and b shows a quick decay of TC concentration with electrolysis time in both, EF-BDD and EF-Pt configurations. The antibiotic was completely removed at 15, 12 and 10 min for 0.5, 2.0 and 1.0 g L^{-1}, respectively, by EF-Pt/Chalcopyrite, whereas for EF-BDD/Chalcopyrite, it disappeared at slightly shorter times (12, 10 and 7 min) for the same catalyst dosage. TC can be efficiently oxidized by homogeneous •OH generated in the bulk solution

Table 2
Pseudo-first-order rate constants and square of the linear regression coefficients for 0.20 mM TC decays during EF/Chalcopyrite.

Cell	[TC] (mM)	[Chalcopyrite] (g L^{-1})	I (mA)	$k_{app,TC}$ (min^{-1})	R^2
BDD/carbon-felt	0.20	0.5	300	0.470 ± 0.016	0.987
		1.0		**0.907 ± 0.012**	0.982
		2.0		0.670 ± 0.023	0.980
		1.0	50	0.324 ± 0.012	0.993
			100	0.460 ± 0.013	0.989
			200	0.580 ± 0.012	0.983
			300	0.907 ± 0.031	0.982
			500	0.950 ± 0.008	0.981
Pt/carbon-felt	0.20	0.5	300	0.144 ± 0.004	0.980
		1.0		**0.401 ± 0.010**	0.984
		2.0		0.247 ± 0.003	0.980
		1.0	50	0.098 ± 0.001	0.993
			100	0.146 ± 0.004	0.983
			200	0.178 ± 0.004	0.980
			300	0.401 ± 0.015	0.984
			500	0.694 ± 0.011	0.989

from Fenton's reaction (2) and Fenton-like reaction (13), and heterogeneous BDD(•OH) produced at the anode surface from water oxidation (1). Better results with BDD anode can be explained by its high oxidation power compared to Pt anode, due to its greater O_2 evolution overvoltage and lower physisorption of BDD(•OH) that are easily available. In contrast, Pt anode exhibits relatively smaller O_2 overvoltage, with Pt(•OH) chemisorbed at the anode surface that are less available for oxidation of organics.

As can be seen in the inset panels of Fig. 3a and b, TC oxidation rate increased with initial chalcopyrite concentration from 0.5 to 1.0 g L^{-1}, but decreased when using 2.0 g L^{-1}. Note that under all conditions, degradation kinetics well fitted a pseudo-first-order reaction and kinetic analysis of the curves in Fig. 3 is summarized in Table 2. These results imply that Fe^{2+} and Cu^{2+} generation is a rate limiting step during TC oxidation in EF/Chalcopyrite process. As chalcopyrite dosage increases, Fe^{2+} and Cu^{2+} concentrations released from chalcopyrite surface are enhanced, leading to a rise of •OH formation from Reactions (2) and (13), whence accelerating TC degradation rate. However, further increase in the amount of catalyst was detrimental as the kinetic rate of the •OH wasting reactions with Fe^{2+} (Reaction (15)) and with and Cu^{+} (Reaction (16)) is increased. 1.0 g L^{-1} was thus the dosage chosen for the rest of the experiments.

$$Fe^{2+} + {}^{\bullet}OH \rightarrow Fe^{3+} + OH^{-} \quad (15)$$

$$Cu^{+} + {}^{\bullet}OH \rightarrow Cu^{2+} + OH^{-} \quad (16)$$

3.3. *Effect of current on the decay kinetics of TC*

A key parameter affecting the oxidation efficiency of EF process is the applied current, since it is responsible for the regulation of the amounts of generated •OH from Reactions (1), (3) and (10), and M(•OH) production from Reaction (4). The influence of applied current was assessed for the treatment of 230 mL of 0.20 mM TC in 0.050 M Na_2SO_4 with 1.0 g L^{-1} of chalcopyrite concentration.

Fig. 4a and b shows the decay in TC concentration using BDD/carbon-felt and Pt/carbon-felt cells, respectively, at different current values. The drug was completely removed at 5, 7, 10, 11 and 12 min for 500, 300, 200, 100 and 50 mA by EF-BDD/Chalcopyrite process, whereas for EF-Pt/Chalcopyrite it disappeared at slightly longer times of 7, 10, 12, 20 and 25 min for the same current values. This means that TC oxidation rate is risen up as current grows, owing to the greater amounts of •OH formed from Fenton's reaction (2), Fenton-like reaction (13) and water discharge at the anode surface (4), as a consequence of an increase of current applied. BDD anodes are known to enhance the effectiveness of the EF process due to the parallel oxidation of organics at the anode surface by "physisorbed" BDD(•OH) generated according to Reaction (4) [10,19,20]. This fact accounts for the higher degradation rates obtained when using a BDD electrode, as mentioned in the previous section.

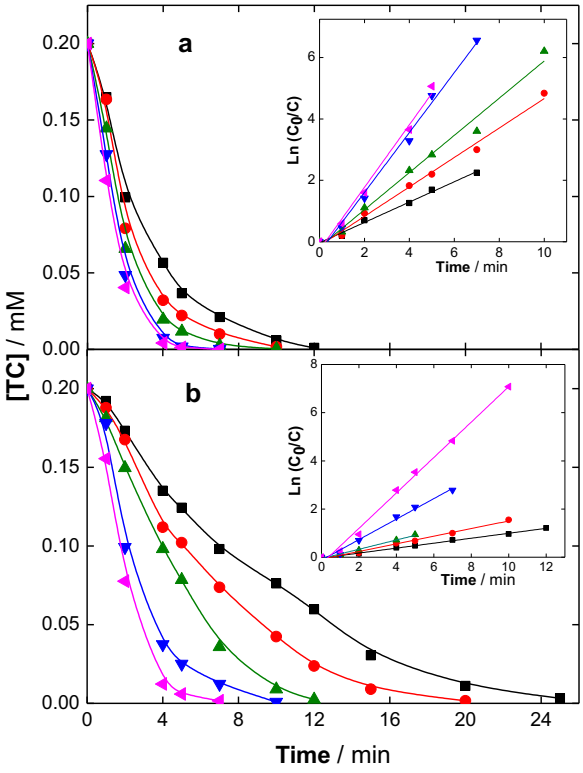

Fig. 4. Effect of current on the concentration decay of TC with electrolysis time for the EF/Chalcopyrite treatment of 230 mL solutions containing 0.20 mM substrate, 0.050 M Na_2SO_4 and 1.0 g L^{-1} chalcopyrite at 25 °C using (a) BDD/carbon-felt and (b) Pt/carbon-felt cells. Applied current (mA): (■) 50, (●) 100, (▲) 200, (▼) 300 and (◀) 500. Inset panels show the kinetic analysis considering a pseudo-first-order reaction between TC and •OH.

The decay on TC concentration was again analysed by simple first-order kinetic equations (Fig. 4a and b). The pseudo-first-order rate constants $k_{app,TC}$ and the corresponding linear regression coefficients (R^2) are also presented in Table 2. Based on the above mentioned kinetic model, the absolute (second order) rate constant ($k_{abs(TC)}$) for the hydroxylation reaction of TC was also determined. The competition kinetic method was applied using *p*-hydroxybenzoic acid (HBA) as standard competitor, with

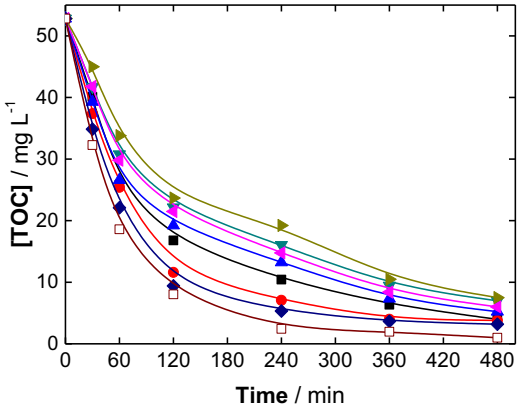

Fig. 5. TOC removal vs. electrolysis time for EF treatment of 230 mL solutions containing 0.20 mM TC in 0.050 M Na_2SO_4 at 300 mA, using an undivided BDD/carbon-felt cell at room temperature with: (■) 0.10 mM Cu^{2+} + 0.20 mM Fe^{2+}; (●) 0.20 mM Cu^{2+} + 0.20 mM Fe^{2+}; (▲) 0.50 mM Cu^{2+} + 0.20 mM Fe^{2+}; (▼) 0.10 mM Cu^{2+}; (◀) 0.20 mM Cu^{2+}; (▶) 0.50 mM Cu^{2+}; (♦) 0.20 mM Fe^{2+} and (□) 1.0 g L^{-1} chalcopyrite.

a well-known absolute rate constant of its oxidation reaction with •OH: $k_{abs(HBA)} = 2.19 \times 10^9$ M^{-1} s^{-1} [37]. A solution containing the same 0.20 mM concentration of both, TC and HBA, were degraded under EF/Chalcopyrite conditions. The absolute rate constant was then calculated from Eq. (17), resulting to be $k_{abs(TC)} = 3.19 \times 10^9$ M^{-1} s^{-1}:

$$k_{abs(TC)} = k_{abs(HBA)} \frac{k_{app,TC}}{k_{app,p-HBA}} \quad (17)$$

3.4. Combination of Cu^{2+} and Fe^{2+} to catalyze oxidation of TC and comparison with EF/Chalcopyrite process

The nature and concentration of the catalyst is crucial in Fenton's reaction chemistry [7,12,34]. Hence, the synergistic effect of both metal ions as catalysts on the degradation of 0.20 mM TC by EF process using the BDD/carbon-felt cell was investigated. Fig. 5 presents the effect of Cu^{2+} concentration (in the range of 0.10–0.50 mM) on TOC decay, as well as the effect of three mixed solutions containing 0.10 mM Cu^{2+} + 0.20 mM Fe^{2+}, 0.20 mM Cu^{2+} + 0.20 mM Fe^{2+} and 0.50 mM Cu^{2+} + 0.20 mM Fe^{2+}. It can be seen that after 240 min of electrolysis, solution TOC was reduced to 64 ± 0.210%, 70 ± 0.152% and 72 ± 0.151% for 0.10, 0.20 and 0.50 mM Cu^{2+}, respectively. On the other hand, TOC removal was 75 ± 0.438%, 80 ± 0.509% and 87 ± 0.298% when the catalyst was formed from a mixture of 0.20 mM Fe^{2+} and 0.10, 0.20 and 0.50 mM Cu^{2+}, respectively, whereas mineralization rate was better when using 0.20 mM Fe^{2+} alone (90 ± 0.040%) or 1.0 g L^{-1} chalcopyrite (95 ± 0.084%). As expected, mineralization kinetics are slower when using only Cu^{2+} ions, which can be related to the decrease in their concentration, as they can be reduced at the cathode surface, resulting in deposition of elemental Cu^0 [23] and thus deactivating part of the cathode surface. Moreover, high amounts of Cu^{2+} were detrimental, which is due to •OH consumption with an excess of Cu^+ ions (Reaction (16)), as in the case of Fe^{2+}. On the other hand, the presence of both, Fe^{2+} and Cu^{2+} ions, showed a positive synergistic effect, accelerating the mineralization kinetic rates. The best TOC decay rate for a Fe^{2+}/Cu^{2+} mixture was that of the equimolar 0.20 mM concentration. It is worth noting that even if the mineralization rate of the 0.20 mM Fe^{2+}/Cu^{2+} mixture presented no significant difference with that corresponding to the use of Fe^{2+} ions in the absence of Cu^{2+}, the use of chalcopyrite gave the greater TOC decay rate, which can be explained by the equilibrium attained by the series of Reactions (5)–(7), which provides the most favourable conditions

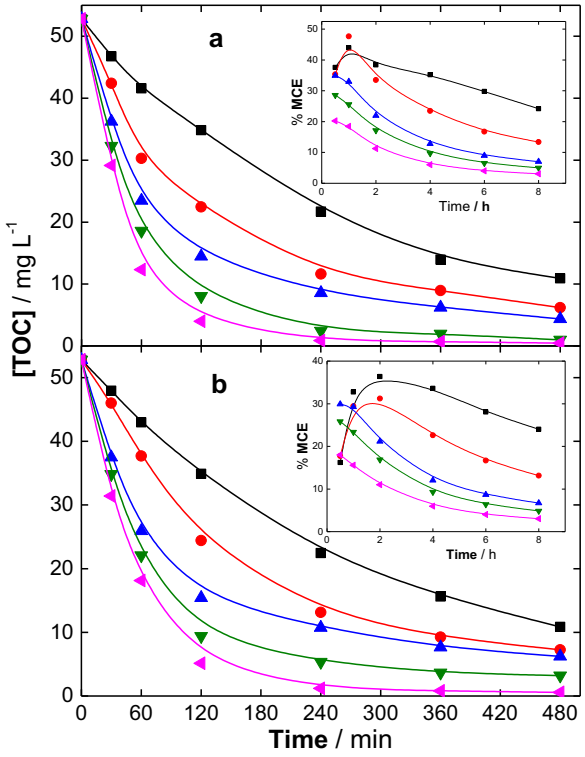

Fig. 6. Percentage of TOC removal vs. electrolysis time for: (a) EF/Chalcopyrite with 1.0 g L^{-1} chalcopyrite concentration and (b) EF with 0.20 mM Fe^{2+}, for 230 mL of 0.20 mM TC solutions in 0.050 M Na_2SO_4 at pH 3.0 and room temperature, using a BDD/carbon-felt cell at: (■) 50 mA, (●) 100 mA, (▲) 200 mA, (▼) 300 mA and (◀) 500 mA. The inset panels show the corresponding mineralization current efficiencies (MCE).

for the catalysis of Fenton's reaction. In fact, the beneficial synergistic effect of the couple Fe^{2+}/Cu^{2+} has been previously reported, which has been ascribed to the effective attack of Cu(II)-carboxylate complexes by •OH, whose reaction rate constant is faster than the rate constant of the oxidative attack of Fe(III)-carboxylate complexes by •OH [24,36,38]. Additionally, it has been reported that Cu^{2+} contributes to the generation of •OH through the series of Reactions (11)–(14), along with its reduction with organic radicals R• by Reaction (18) [38]:

$$Cu^{2+} + R^{\bullet} \rightarrow Cu^{+} + R^{+} \quad (18)$$

It is worthy to note that the concentration of Fe^{2+} ions provided by chalcopyrite was always below the concentration of Fe^{2+} used in conventional EF process. Therefore, the higher efficiency of EF/Chalcopyrite is not related to a greater amount of Fe^{2+} released by the mineral. The amount of Fe^{2+} ions released into the solution by 0.50, 1.0 and 2.0 g L^{-1} of chalcopyrite was 0.03, 0.05 and 0.13 mM, respectively, according to ICP analysis.

3.5. EF/chalcopyrite vs conventional EF: comparative assessment

The influence of current intensity on the performance of conventional EF and EF/Chalcopyrite was studied with the aim of comparing both processes. Current values ranging between 50 and 500 mA were applied to electrolysis of 0.20 mM TC solutions using the BDD anode. TOC decay with electrolysis time is presented in Fig. 6a and b, for EF/Chalcopyrite and conventional EF, respectively. TOC removal increased with increasing current from 50 to 500 mA, due to the improved production of both, BDD(•OH) from Reaction (4), and •OH from Reactions (2) and (13), which is a consequence of the greater electrogeneration of H_2O_2 from Reaction (1), as well as

the regeneration of Fe^{2+} from Reaction (3) and Cu^{+} from Reaction (10).

By comparison of both, heterogeneous and homogeneous EF processes (Fig. 6a and b), it can be noted that since the first 120 min of treatment at 50, 100, 200, 300 and 500 mA, TOC was importantly reduced by 33 ± 0.538%, 54 ± 0.881%, 71 ± 0.479%, 82 ± 0.193% and 90 ± 0.156% in EF, respectively, whereas it was reduced by 34 ± 0.361%, 57 ± 0.285%, 72 ± 0.125%, 85 ± 0.283% and 92 ± 0.093% by EF/Chalcopyrite for the same current values. These results point out the slightly better performance of the mineral chalcopyrite as catalyst for the electro-Fenton process. On the other hand, mineralization rates become slower at longer treatment times: after 480 min of EF/Chalcopyrite treatment, 79 ± 0.270%, 88 ± 0.143%, 91 ± 0.057%, 98 ± 0.024% and 99 ± 0.014% of TOC removal was obtained for 50, 100, 200, 300 and 500 mA, respectively, whereas 77 ± 0.304%, 86 ± 0.101%, 88 ± 0.215%, 94 ± 0.095% and 98 ± 0.020% was attained for conventional EF. This trend can be ascribed to the recalcitrance to •OH attack of the short-chain aliphatic by-products formed by oxidative ring opening reactions of aromatic/cyclic intermediates generated during the first stages of electrolysis, as discussed in following sections. The better performance of EF/Chalcopyrite can be related to the self-regulation of the amount of Fe^{2+} and Cu^{2+} ions from chalcopyrite surface throughout electrolysis according to Reactions (5)–(7), which enhances the oxidative destruction of organics by homogeneous •OH in the bulk generated from both, Fenton's reaction (2), and Fenton-like reaction (13). Furthermore, the synergistic effect of Cu^{2+} ions contained in the mineral contributes to the mineralization efficiency, since Cu(II)-carboxylate complexes formed during the oxidative degradation of organics have been reported to be more reactive towards •OH than their homologous Fe(III)-carboxylate complexes, which favours their quicker mineralization [38].

Evolution of MCE values, calculated from Eq. (8), are shown in the inset panels of Fig. 6a and b. In both cases MCE increased at the early stages of treatment, attaining a maximum value, which suggests a rapid mineralization of organic intermediates by the action of •OH/BDD(•OH). On the contrary, the progressive decay of MCE at long electrolysis times is indicative of production of less reactive intermediates, such as short-chain carboxylic acids, which are more difficultly destroyed by BDD(•OH) and/or •OH [39,40]. Slightly higher MCE values were always observed for EF/Chalcopyrite treatment, which is in agreement with the better mineralization rates achieved by this process. After 1 h of electrolysis, the maximum MCE values were 44.0 ± 1.171%, 47.6 ± 0.782%, 33 ± 0.743%, 25.6 ± 0.781% and 18.5 ± 0.437% for EF/Chalcopyrite at 50, 100, 200, 300 and 500 mA, respectively, whereas 32.7 ± 1.011%, 29.4 ± 1.173%, 29.3 ± 0.224%, 23.4 ± 0.340% and 15.6 ± 0.456% were for conventional EF. The dramatic decrease in MCE values at higher treatment times is also a result of the reduced amount of organic matter in the solution and slow oxidation rate of short-chain carboxylic acids.

On the other hand, MCE dropped as current increased, as expected from the concomitant acceleration of •OH parasitic reactions, mainly oxidation of BDD(•OH) to O_2 at the anode surface by Reaction (19), dimerization of •OH to H_2O_2 by Reaction (20), and its reaction with H_2O_2 for the formation the hydroperoxyl radical (HO_2•) following Reaction (21) or with Fe^{2+} and Cu^{+} according to the Reaction (15) and (16), respectively [7,12].

$$2BDD(^{\bullet}OH) \rightarrow 2BDD + O_2 + 2H^{+} + 2e^{-} \quad (19)$$

$$2^{\bullet}OH \rightarrow H_2O_2 \quad (20)$$

$$H_2O_2 + {}^{\bullet}OH \rightarrow HO_2^{\bullet} + H_2O \quad (21)$$

The depletion of MCE has been reported to be generally accompanied by an increase of the energy consumption per unit TOC mass (EC_{TOC}, in kW h (g TOC)$^{-1}$), which is calculated on the basis of the E_{cell} [12]. Consequently, lower EC_{TOC} values are expected by EF/Chalcopyrite as it gave higher MCE than conventional EF.

3.6. Identification of aromatic intermediates and proposed reaction pathway

HPLC–MS was used to identify polar intermediates with high molecular weight formed during EF/Chalcopyrite treatment, while GC–MS after silylation was used for identification of non-polar and polar intermediates with lower molecular weight. Table 3 summarizes all identified by-products formed during EF/Chalcopyrite process.

As expected from the complexity of TC molecule, a great variety of oxidation by-products were formed and then destroyed during electrolysis under EF/Chalcopyrite conditions. The identification of these intermediates allowed proposing the mechanistic pathway of Fig. 7 for TC mineralization by •OH/BDD(•OH), assuming that they are representative of the complicated mixture of degradation compounds. In this way, according to the reactivity of hydroxyl radicals, multiple hydroxylation reactions occurred during the first stages of oxidation, which leads to structures of the kind of product (I), in which addition of •OH to C-2 and C-11a takes place. Further •OH attack to one methyl of the amino group leads to the formation of compound (II). Compounds (III) and (IV) are produced from demethylation reactions resulted from oxidation of the amino group. Similarly, compound (II) can suffer demethylation reactions after decarboxylation at the CH_3-NR- position. Subsequent leakage of aromatic rings, more likely commencing in ring D, yielded to compounds of the kind of (V), whose progressive cleavage produced compounds with lower molecular weight, structures (VI)-(X). Ultimate ring-opening of these cyclic/aromatic intermediates leads to the formation of short-chain carboxylic acids, which are generally reported as the end-products before total mineralization to CO_2, water and inorganic ions [39,40]. This mechanism is in agreement with that proposed by Zhu et al. [41] for the photodegradation of TC using heterogeneous photocatalysis with TiO_2, in which several of the identified by-products coincided with the ones we found. However, some differences arise, mainly in the by-products formed during the first moments of oxidation, where in the case of EF/Chalcopyrite, the pathway goes mostly through multiple hydroxylation reactions and exhaustive demethylations. On the other hand, Dalmazio et al. [42] also reported the formation of compound (I) during the treatment of TC solutions by ozone. Different studies concerning the electrochemical treatment of TC solutions have been reported, however, to the best of our knowledge, its mineralization pathway via electrogenerated •OH has not been presented elsewhere [34,43,44].

3.7. Time-course of generated carboxylic acids with chalcopyrite-EF and conventional-EF using BDD anode

Samples collected during EF/Chalcopyrite were analysed by ion-exclusion HPLC in order to identify and quantify the formed short-chain carboxylic acids. HPLC chromatograms displayed well-defined peaks with following retention times (t_R) ascribed to: oxalic (t_R = 12.0 min), oxamic (t_R = 17.2 min), acetic (t_R = 19.3 min), succinic (t_R = 22 min), malic (t_R = 13.2 min) and malonic (t_R = 9.8 min) acids. The concentration of the above acids was determined via standard compounds and their evolution during electrolysis is depicted in Fig. 8. Malic, malonic and succinic acids can be formed from the cleavage of the benzene ring of aromatics, while oxamic acid can be produced from the degradation of N-derivatives [39,45]. These species form iron-carboxylate and copper-carboxylate complexes that require long destruction times due to their lower reactivity with BDD(•OH) and •OH, hence constituting residual TOC on longer times [11,12]. The species formed in greater amount were

Table 3
Intermediate products identified using HPLC–MS and GC–MS during the degradation of TC by EF/Chalcopyrite process with BDD anode.

Compound	t_R (min)	Molecular mass (g mol^{-1})	Molecular structure	Analytical technique
I	6.60	476	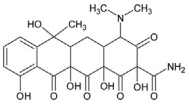	HPLC–MS
II	7.96	490	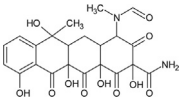	HPLC–MS
III	7.04	430	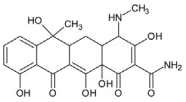	HPLC–MS
IV	9.28	448	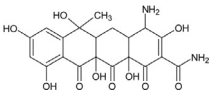	HPLC–MS
V	9.36	450	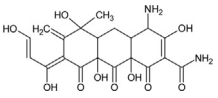	HPLC–MS
VI	12.90	152	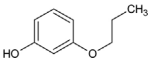	GC–MS[a]
VII	11.40	206	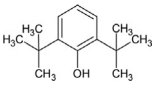	GC–MS[a]
VIII	18.30	223	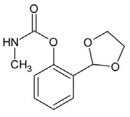	GC–MS[a]
IX	10.82	138		GC–MS[a]
X	11.07	134	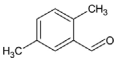	GC–MS[a]
XI	22	118	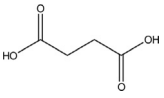	HPLC
XII	13.25	134	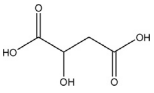	HPLC
XIII	9.80	104	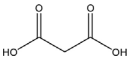	HPLC
XIV	12	90	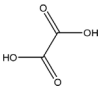	HPLC
XV	17.20	89		HPLC
XVI	19.70	60		HPLC

[a] Identification after derivatization with N,O-Bis (trimethylsilyl) trifluoroacetamide.

oxalic, oxamic and acetic acid, which have been reported to be the end-products before complete mineralization to CO_2.

It is important to notice that oxamic and oxalic acids were more rapidly destroyed when using chalcopyrite, since they disappeared after 240 and 360 min, respectively, being both compounds were detected after 8 h in conventional EF process (Fig. 8). This behaviour can be accounted for by the presence of Cu^{+2} ions, whose carboxylate complexes have shown to be more reactive towards •OH and

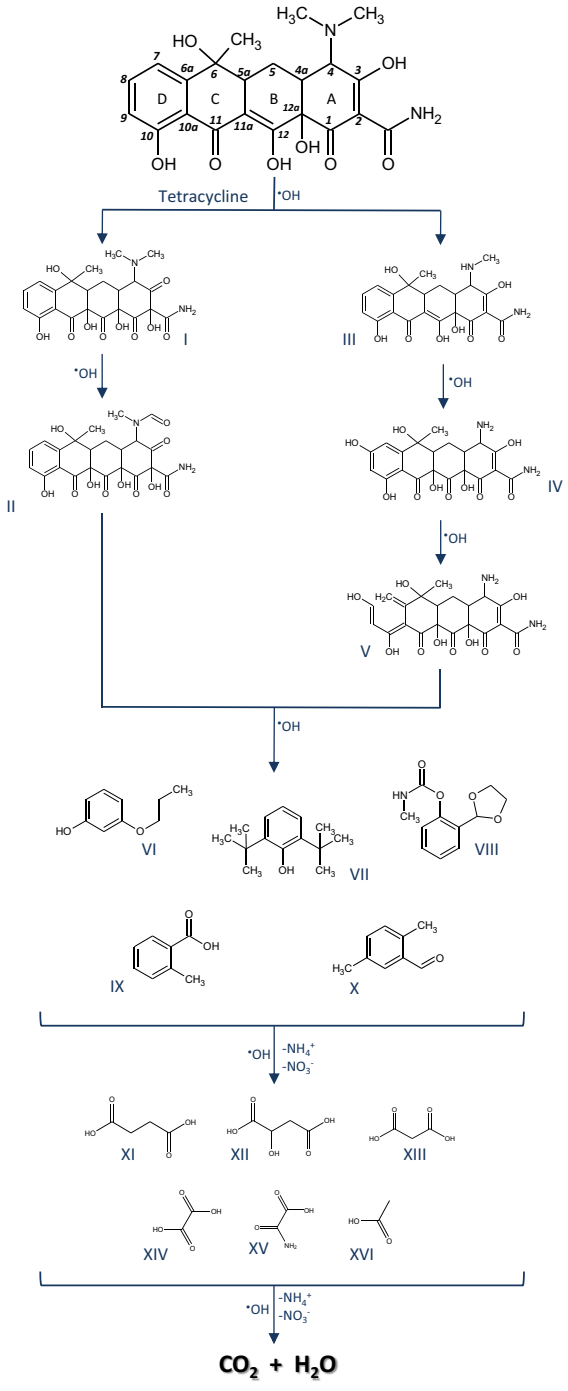

Fig. 7. Proposed reaction pathway of TC mineralization by EF/Chalcopyrite process. Only the action of homogeneous •OH as main oxidant is considered for sake of simplicity, even if organics can also be destroyed by heterogeneous BDD(•OH) at the BDD surface.

provoke an increment on their oxidation rate [38], as discussed in Section 3.5. Respecting acetic acid, it was faster removed during conventional EF, nonetheless, not significant levels were detected after 8 h of both, homogeneous- and chalcopyrite-EF processes.

3.8. Identification and evolution of inorganic ions

The fate of the initial N atom of TC during EF/Chalcopyrite in both, BDD/carbon-felt and Pt/carbon-felt cells at 300 mA, was investigated. Fig. 9 shows the trials concerning NH_4^+ and NO_3^- ions

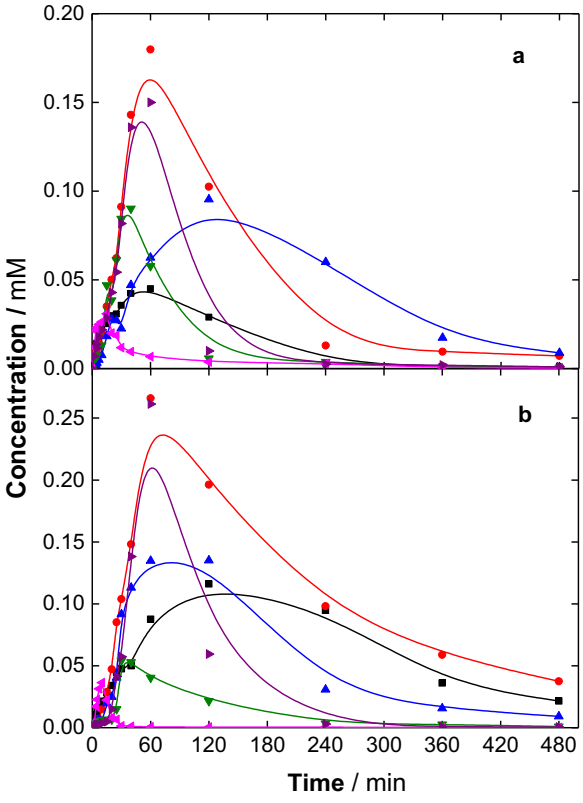

Fig. 8. Time course of carboxylic acids generated during (a) EF/Chalcopyrite with 1.0 g L^{-1} and (b) conventional-EF with 0.20 mM Fe^{2+}, of 0.20 mM TC solutions in 0.050 M Na_2SO_4 at 300 mA and room temperature using an undivided BDD/carbon-felt cell. (●) oxalic, (■) oxamic, (▲) acetic, (▼) succinic, (◀) malic and (▶) malonic acids.

determined by ionic chromatography. No other inorganic nitrogen ions such as NO_2^- were detected. It can be observed that NH_4^+ ion was accumulated in larger extent than NO_3^- ion in both cells, which is in agreement with what was proposed in Reaction (9). Contents of 0.230 ± 0.006 mM NH_4^+ (57.5% of initial N) and 0.044 ± 0.001 mM NO_3^- (11.0% of initial N) were accumulated after 480 min with EF/Chalcopyrite with Pt anode, whereas 0.300 ± 0.009 mM NH_4^+ (75.0% of initial N) and 0.017 ± 0.001 mM NO_3^- (4.2% of initial N) were found in the case of EF/Chalcopyrite with BDD anode. These results confirm the higher mineralization rates obtained when utilizing a BDD anode. On the other hand, the drop in NO_3^- content after the maximum peak at 120 min in the case of the BDD cell evidences the oxidation and reduction of these ions into volatile compounds, such as N_2 and N_xO_y, a behaviour that has been previously stated [46,47].

4. Conclusions

An innovative heterogeneous electro-Fenton process catalysed by the natural mineral chalcopyrite, "EF/Chalcopyrite process", was successfully applied for the degradation and mineralization of TC aqueous solutions. This "green" process presents two remarkable advantages: firstly, the utilization of low cost and reusable solid catalyst as source of Fe^{2+} and Cu^{2+} ions, and secondly, the capacity of performing the EF process at natural pH, since chalcopyrite provides the optimal pH value of about 3.0 for the Fenton's reaction. A comparison with the conventional EF process demonstrated that besides the enhanced sustainability of EF/Chalcopyrite, it also showed a slightly superior performance, which was ascribed to the self-regulation of Fe^{2+} and Cu^{2+} content in the reaction medium, exerting a synergistic effect.

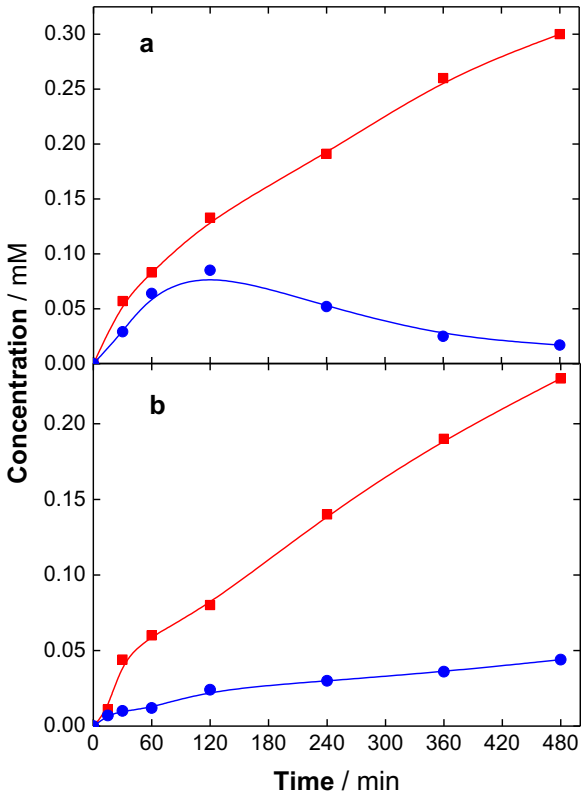

Fig. 9. Time-course of inorganic ions NH_4^+ (■) and NO_3^- (●) released during EF/Chalcopyrite treatment of 0.20 mM of TC solutions in 0.050 M Na_2SO_4 containing 1.0 g L^{-1} chalcopyrite, at 300 mA and room temperature using (a) BDD/carbon felt and (b) Pt/carbon-felt cells.

Based on the overall results, 1.0 g L^{-1} of chalcopyrite and 300 mA current using a BDD anode are the optimal conditions for the degradation/mineralization of TC solutions, achieving 85% and 98% of TOC removal at 2 and 8 h, respectively. It is worthy to note that high mineralization rates were obtained during the first 2 h of electrolysis. At this time, MCE was at most favourable levels. These results suggest that EF/Chalcopyrite at short treatment times could be integrated in sequential processes with conventional methods (mainly biological) for practical applications.

The concentration decay of TC always obeyed pseudo-first-order kinetics and the absolute rate constant of its reaction with •OH was determined to be 3.19×10^9 M^{-1} s^{-1} Quasi-total mineralization of the drug solutions (98%) was achieved after 360 min under optimized conditions of EF/Chalcopyrite. Furthermore, detoxification of TC solutions was also achieved, whence demonstrating the effectiveness of this heterogeneous EF process for destroying toxic intermediates. The identification of several intermediates allowed proposing a degradation pathway for the mineralization of TC with •OH.

These findings demonstrate the potentiality of using natural products as heterogeneous catalyst for EF process, which constitutes significant advantages as stated above. Moreover, the synergistic effects of Cu^{2+} ions were pointed out, stimulating further investigation on the use of different transition metals as co-catalysts for enhancing the performance of heterogeneous EF/Chalcopyrite process.

References

[1] A. Küster, N. Adler, Pharmaceuticals in the environment: scientific evidence of risks and its regulation, Philos. Trans. R. Soc. Lond. B. Biol. Sci. 369 (2014) 20130587.
[2] A.R. Ribeiro, O.C. Nunes, M.F.R. Pereira, A.M.T. Silva, An overview on the advanced oxidation processes applied for the treatment of water pollutants defined in the recently launched Directive 2013/39/EU, Environ. Int. 75 (2015) 33–51.
[3] S.A. Ortiz de García, G. Pinto Pinto, P.A. García-Encina, R. Irusta-Mata, Ecotoxicity and environmental risk assessment of pharmaceuticals and personal care products in aquatic environments and wastewater treatment plants, Ecotoxicology 23 (2014) 1517–1533.
[4] I.T. Carvalho, L. Santos, Antibiotics in the aquatic environments: a review of the European scenario, Environ. Int. 94 (2016) 736–757.
[5] K. Kümmerer, Antibiotics in the aquatic environment—a review—part I, Chemosphere 75 (2009) 417–434.
[6] H. Dong, X. Yuan, W. Wang, Z. Qiang, Occurrence and removal of antibiotics in ecological and conventional wastewater treatment processes: a field study, J. Environ. Manage. 178 (2016) 11–19.
[7] M.A. Oturan, J.J. Aaron, Advanced oxidation processes in water/wastewater treatment: principles and applications. A review, Crit. Rev. Environ. Sci. Technol. 44 (2014) 2577–2641.
[8] I.O. Uribe, A. Mosquera-Corral, J.L. Rodicio, S. Esplugas, Advanced technologies for water treatment and reuse, AIChE J. 61 (2015) 3146–3158.
[9] I. Sirés, E. Brillas, M.A. Oturan, M.A. Rodrigo, M. Panizza, Electrochemical advanced oxidation processes: today and tomorrow. A review, Environ. Sci. Pollut. Res. 21 (2014) 8336–8367.
[10] C.A. Martínez-Huitle, M.A. Rodrigo, I. Sirés, O. Scialdone, Single and coupled electrochemical processes and reactors for the abatement of organic water pollutants: a critical review, Chem. Rev. 115 (2015) 13362–13407.
[11] E. Brillas, C.A. Martínez-Huitle, Decontamination of wastewaters containing synthetic organic dyes by electrochemical methods. An updated review, Appl. Catal. B: Environ. 166 (2015) 603–643.
[12] E. Brillas, I. Sirés, M.A. Oturan, Electro-Fenton process and related electrochemical technologies based on Fenton's reaction chemistry, Chem. Rev. 109 (2009) 6570–6631.
[13] A. Özcan, A. Atılır Özcan, Y. Demirci, Evaluation of mineralization kinetics and pathway of norfloxacin removal from water by electro-Fenton treatment, Chem. Eng. J. 304 (2016) 518–526.
[14] E. Mousset, Z. Wang, J. Hammaker, O. Lefebvre, Physico-chemical properties of pristine graphene and its performance as electrode material for electro-Fenton treatment of wastewater, Electrochim. Acta 214 (2016) 217–230.
[15] M.S. Çelebi, N. Oturan, H. Zazou, M. Hamdani, M.A. Oturan, Electrochemical oxidation of carbaryl on platinum and boron-doped diamond anodes using electro-Fenton technology, Sep. Purif. Technol. 156 (2015) 996–1002.
[16] K. Cruz-González, O. Torres-López, A. García-León, J.L. Guzmán-Mar, L.H. Reyes, A. Hernández-Ramírez, J.M. Peralta-Hernández, Determination of optimum operating parameters for Acid Yellow 36 decolorization by electro-Fenton process using BDD cathode, Chem. Eng. J. 160 (2010) 199–206.
[17] R.D.C. Soltani, A. Rezaee, A.R. Khataee, H. Godini, Electrochemical generation of hydrogen peroxide using carbon black-, carbon nanotube-, and carbon black/carbon nanotube-coated gas-diffusion cathodes: effect of operational parameters and decolorization study, Res. Chem. Intermed. 39 (2013) 4277–4286.
[18] H. Lan, W. He, A. Wang, R. Liu, H. Liu, J. Qu, C.P. Huang, An activated carbon fiber cathode for the degradation of glyphosate in aqueous solutions by the electro-Fenton mode: optimal operational conditions and the deposition of iron on cathode on electrode reusability, Water Res. 105 (2016) 575–582.
[19] F. Sopaj, N. Oturan, J. Pinson, F. Podvorica, M.A. Oturan, Effect of the anode materials on the efficiency of the electro-Fenton process for the mineralization of the antibiotic sulfamethazine, Appl. Catal. B: Environ. 199 (2016) 331–341.
[20] N. Oturan, E. Brillas, M.A. Oturan, Unprecedented total mineralization of atrazine and cyanuric acid by anodic oxidation and electro-Fenton with a boron-doped diamond anode, Environ. Chem. Lett. 10 (2012) 165–170.
[21] S. Garcia-Segura, E. Vieira dos Santos, C.A. Martínez-Huitle, Role of sp^3/sp^2 ratio on the electrocatalytic properties of boron-doped diamond electrodes: a mini review, Electrochem. Commun. 59 (2015) 52–55.
[22] A. Kapałka, G. Fóti, C. Comninellis, The importance of electrode material in environmental electrochemistry: formation and reactivity of free hydroxyl radicals on boron-doped diamond electrodes, Electrochim. Acta 54 (2009) 2018–2023.
[23] M. Pimentel, N. Oturan, M. Dezotti, M.A. Oturan, Phenol degradation by advanced electrochemical oxidation process electro-Fenton using a carbon felt cathode, Appl. Catal. B: Environ. 83 (2008) 140–149.
[24] S. Garcia-Segura, E. Brillas, L. Cornejo-Ponce, R. Salazar, Effect of the Fe^{3+}/Cu^{2+} ratio on the removal of the recalcitrant oxalic and oxamic acids by electro-Fenton and solar photoelectro-Fenton, Sol. Energy 124 (2016) 242–253.
[25] S. Ammar, M.A. Oturan, L. Labiadh, A. Guersalli, R. Abdelhedi, N. Oturan, E. Brillas, Degradation of tyrosol by a novel electro-Fenton process using pyrite as heterogeneous source of iron catalyst, Water Res. 74 (2015) 77–87.
[26] N. Barhoumi, N. Oturan, H. Olvera-Vargas, E. Brillas, A. Gadri, S. Ammar, M.A. Oturan, Pyrite as a sustainable catalyst in electro-Fenton process for improving oxidation of sulfamethazine. Kinetics, mechanism and toxicity assessment, Water Res. 94 (2016) 52–61.
[27] G.-D. Fang, D.D. Dionysiou, S.R. Al-Abed, D.-M. Zhou, Superoxide radical driving the activation of persulfate by magnetite nanoparticles: implications for the degradation of PCBs, Appl. Catal. B: Environ. 129 (2013) 325–332.

[28] E. Expoísito, C.M. Saínchez-Saínchez, V. Montiel, Mineral iron oxides as iron source in electro-Fenton and photoelectro-Fenton mineralization processes, J. Electrochem. Soc. 154 (2007) E116–E122.
[29] W. Zeng, G. Qiu, H. Zhou, M. Chen, Electrochemical behaviour of massive chalcopyrite electrodes bioleached by moderately thermophilic microorganisms at 48 °C, Hydrometallurgy 105 (2011) 259–263.
[30] Y. Li, N. Kawashima, J. Li, A.P. Chandra, A.R. Gerson, A review of the structure, and fundamental mechanisms and kinetics of the leaching of chalcopyrite, Adv. Colloid Interface Sci. 197 (2013) 1–32.
[31] D. Belkheiri, F. Fourcade, F. Geneste, D. Floner, H. Aït-Amar, A. Amrane, Combined process for removal of tetracycline antibiotic—coupling pre-treatment with a nickel-modified graphite felt electrode and a biological treatment, Int. Biodeterior. Biodegrad. 103 (2015) 147–153.
[32] D. Liang, J. Li, G. Pang, A degradation column for organic dyes based on a composite of $CuFeS_2$ nanocrystals and sawdust, J. Mater. Sci. 51 (2016) 5412–5420.
[33] D. Majuste, V.S.T. Ciminelli, P.J. Eng, K. Osseo-Asare, Applications of in situ synchrotron XRD in hydrometallurgy: literature review and investigation of chalcopyrite dissolution, Hydrometallurgy 131 (2013) 54–66.
[34] N. Oturan, J. Wu, H. Zhang, V.K. Sharma, M.A. Oturan, Electrocatalytic destruction of the antibiotic tetracycline in aqueous medium by electrochemical advanced oxidation processes: effect of electrode materials, Appl. Catal. B: Environ. 140–141 (2013) 92–97.
[35] T.-S. Chen, R.-W. Tsai, Y.-S. Chen, K.-L. Huang, Electrochemical degradation of tetracycline on BDD in aqueous solutions, Int. J. Electrochem. Sci. 9 (2014) 8422–8434.
[36] S. Garcia-Segura, R. Salazar, E. Brillas, Mineralization of phthalic acid by solar photoelectro-Fenton with a stirred boron-doped diamond/air-diffusion tank reactor: influence of Fe^{3+} and Cu^{2+} catalysts and identification of oxidation products, Electrochim. Acta 113 (2013) 609–619.
[37] J. Beltran De Heredia, J. Torregrosa, J.R. Dominguez, J.A. Peres, Kinetic model for phenolic compound oxidation by Fenton's reagent, Chemosphere 45 (2001) 85–90.
[38] R. Salazar, E. Brillas, I. Sirés, Finding the best Fe^{2+}/Cu^{2+} combination for the solar photoelectro-Fenton treatment of simulated wastewater containing the industrial textile dye Disperse Blue 3, Appl. Catal. B: Environ. 115–116 (2012) 107–116.
[39] M.A. Oturan, M. Pimentel, N. Oturan, I. Sirés, Reaction sequence for the mineralization of the short-chain carboxylic acids usually formed upon cleavage of aromatics during electrochemical Fenton treatment, Electrochim. Acta 54 (2008) 173–182.
[40] S. Garcia-Segura, E. Brillas, Mineralization of the recalcitrant oxalic and oxamic acids by electrochemical advanced oxidation processes using a boron-doped diamond anode, Water Res. 45 (2011) 2975–2984.
[41] X.-D. Zhu, Y.-J. Wang, R.-J. Sun, D.-M. Zhou, Photocatalytic degradation of tetracycline in aqueous solution by nanosized TiO_2, Chemosphere 92 (2013) 925–932.
[42] I. Dalmázio, M.O. Almeida, R. Augusti, T.M.A. Alves, Monitoring the degradation of tetracycline by ozone in aqueous medium via atmospheric pressure ionization mass spectrometry, J. Am. Soc. Mass Spectrom. 18 (2007) 679–687.
[43] C.I. Brinzila, N. Monteiro, M.J. Pacheco, L. Ciríaco, I. Siminiceanu, A. Lopes, Degradation of tetracycline at a boron-doped diamond anode: influence of initial pH, applied current intensity and electrolyte, Environ. Sci. Pollut. Res. 21 (2014) 8457–8465.
[44] C.I. Brinzila, M.J. Pacheco, L. Ciríaco, R.C. Ciobanu, A. Lopes, Electrodegradation of tetracycline on BDD anode, Chem. Eng. J. 209 (2012) 54–61.
[45] X. Florenza, A.M.S. Solano, F. Centellas, C.A. Martínez-Huitle, E. Brillas, S. Garcia-Segura, Degradation of the azo dye Acid Red 1 by anodic oxidation and indirect electrochemical processes based on Fenton's reaction chemistry. Relationship between decolorization, mineralization and products, Electrochim. Acta 142 (2014) 276–288.
[46] W.T. Mook, M.H. Chakrabarti, M.K. Aroua, G.M.A. Khan, B.S. Ali, M.S. Islam, M.A. Abu Hassan, Removal of total ammonia nitrogen (TAN), nitrate and total organic carbon (TOC) from aquaculture wastewater using electrochemical technology: a review, Desalination 285 (2012) 1–13.
[47] H. Olvera-Vargas, N. Oturan, D. Buisson, E.D. van Hullebusch, M.A. Oturan, Electro-oxidation of the pharmaceutical furosemide: kinetics, mechanism, and by-products, Clean–Soil Air Water 43 (2015) 1455–1463.